Chapter 11

120° Phase Difference Interference Technology Based on 3 × 3 Coupler and its Application in Laser Noise Measurement

Yang Fei, Xu Dan, Cai Haiwen and Qu Ronghui

Additional information is available at the end of the chapter

http://dx.doi.org/10.5772/66129

Abstract

A 120° phase difference interferometer technology based on an unbalanced Michelson interferometer composed of a 3 × 3 optical fiber coupler is proposed, and based on this technology, the differential phase of the input laser can be obtained. This technology has many applications. This paper introduced its application in laser phase and frequency noise measurement in detail. The relations and differences of the power spectral density (PSD) of differential phase and frequency fluctuation, instantaneous phase and frequency fluctuation, phase noise, and linewidth are derived strictly and discussed carefully. The noise features of some narrow-linewidth lasers are also obtained conveniently without any specific assumptions or noise models. Finally, the application of this technology in the phase-sensitive optical time domain reflectometer (φ-OTDR) is also introduced briefly.

Keywords: interferometer, 120° phase difference, 3 × 3 optical fiber coupler, laser noise measurement, phase-sensitive optical time domain reflectometer

1. Introduction

Single-frequency narrow-linewidth lasers are fundamental to a vast array of applications in fields including metrology, optical frequency transfer, coherent optical communications, high-resolution sensing, and light detection and ranging (LIDAR) [1–9]. In these applications, the phase and frequency noise is one of the key factors to affect the system performance. The characterization and measurement of the phase and frequency noise are very important for the applications, and thus have been one of the most attractive subjects of researches in laser

and photonics field. The phase and frequency noise of such lasers can be conveniently described either in terms of linewidth or in terms of the power spectral density (PSD) of their phase or frequency noise. The linewidth gives a basic and concise parameter for characterizing laser coherence but lacks detailed information on frequency noise and its Fourier frequency spectrum, which is needed for understanding the noise origins and improving laser performances. Therefore, the measurement of frequency noise PSD is a focus of attention in the field, especially for lasers of very high coherence, whose linewidth is not easy to be measured.

To measure the phase and frequency noise, many methods have been proposed, such as beat note method [10], recirculating delayed self-heterodyne (DSH) method [11], DSH technique based on Mach-Zehnder interferometer with 2 × 2 coupler [12, 13], or Michelson interferometer (MI) with 2 × 2 coupler [14]. These methods can obtain good measurement results but need some strict conditions. The beat note method needs a high coherent source as a reference. The recirculating DSH method needs very long fiber delay lines. The DSH interferometers with 2 × 2 coupler need to control the quadrature point by some active feedback methods and accurate calibration.

To overcome these difficulties, we introduce a robust technique that can demodulate directly the laser differential phase accumulated in a delay time and then derive strict mathematical relations between the laser differential phase and the laser phase noise or frequency noise that can describe the complete information on laser phase and frequency noise. Because 3 × 3 optical fiber coupler acts as a 120° optical hybrid, it can demodulate the differential phase of the input light and has been used for DxPSK signal demodulation [15], optical sensors [16], optical field reconstruction, and dynamical spectrum measurement [17]. In this chapter, 120° phase difference interference technology based on an unbalanced Michelson interferometer, which is composed of a 3 × 3 optical fiber coupler and two Faraday rotator mirrors, is utilized to demodulate the differential phase of a laser. The structure has the advantage of being polarization insensitive and adjust-free. Especially, it does not need any active controlling operation that is used in the DSH methods with 2 × 2 coupler. Furthermore, based on the differential phase and strict physical and mathematical derivation, the PSD of the differential phase fluctuation and frequency fluctuation, the PSD of the instantaneous phase fluctuation and frequency fluctuation, laser phase noise, and linewidth are completely calculated and discussed.

2. 120° phase difference interference technology

2.1. Symmetric 3 × 3 optical fiber coupler

Figure 1 shows the schematic diagram of the proposed 120° phase difference technology. As we know, the interferometric signals are 180° out of phase because of 2 × 2 optical fiber coupler. In an ideal 3 × 3 optical fiber coupler, there is a 120° phase difference between any two of the three output ports. A symmetric 3 × 3 optical fiber coupler is described by the matrix.

http://dx.doi.org/10.5772/66129

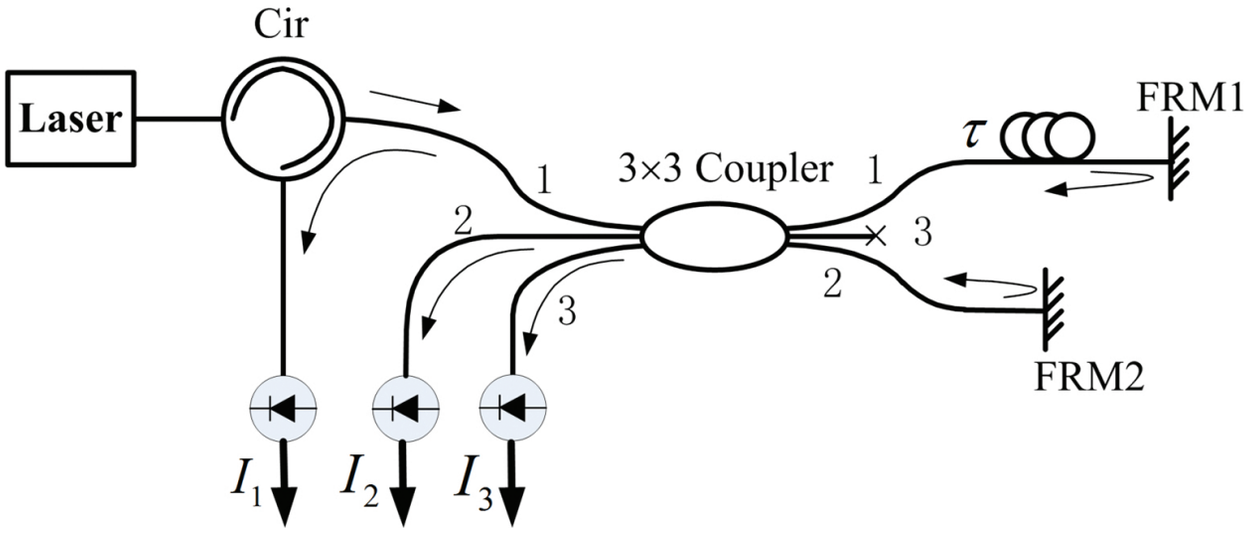

Figure 1. Schematic diagram of the proposed 120° phase difference technology.

$$T_3 = \frac{1}{\sqrt{3}} \begin{pmatrix} 1 & \exp\frac{i2\pi}{3} & \exp\frac{i2\pi}{3} \\ \exp\frac{i2\pi}{3} & 1 & \exp\frac{i2\pi}{3} \\ \exp\frac{i2\pi}{3} & \exp\frac{i2\pi}{3} & 1 \end{pmatrix} \tag{1}$$

The matrix of the two arms of the Michelson interferometer is given by,

$$P = \begin{pmatrix} \exp(i\varphi_1) & 0 & 0 \\ 0 & \exp(i\varphi_2) & 0 \\ 0 & 0 & 0 \end{pmatrix} = \begin{pmatrix} 1 & 0 & 0 \\ 0 & \exp(i\Delta\varphi) & 0 \\ 0 & 0 & 0 \end{pmatrix} \exp(i\varphi_1) \tag{2}$$

Where $\Delta\varphi = \varphi_2 - \varphi_1 = 2\pi n\Delta L/\lambda$ is the phase difference of the two arms of the Michelson interferometer, n is the refractive index of fiber, λ is the wavelength of transmit light, ΔL is the length difference of the two arms. Setting $2\pi/3 = \theta$, the operation of the whole interferometer is then described by the system matrix.

$$M = T_3 P T_3 = \frac{e^{i\varphi_1}}{3} \begin{pmatrix} 1+e^{i(\Delta\varphi+2\theta)} & (1+e^{i\Delta\varphi})e^{i\theta} & e^{i\theta}(1+e^{i(\Delta\varphi+\theta)}) \\ e^{i\theta}(1+e^{i\Delta\varphi}) & e^{i2\theta}+e^{i\Delta\varphi} & e^{i\theta}(e^{i\theta}+e^{i\Delta\varphi}) \\ e^{i\theta}(1+e^{i(\Delta\varphi+\theta)}) & e^{i\theta}(e^{i\theta}+e^{i\Delta\varphi}) & e^{i2\theta}(1+e^{i\Delta\varphi}) \end{pmatrix} \tag{3}$$

The electric field of input laser is expressed by,

$$E(t) = |E(t)| \exp[i\omega_0 t + i\varphi(t)] \tag{4}$$

with amplitude $|E(t)|$, center frequency ω_0, and instantaneous phase fluctuation $\varphi(t)$. The input field $K^{in} = [E(t), 0, 0]^T$ is a vector whose elements are the amplitudes of the input modes to the interferometer. K^{in} is transformed by the interferometer into an output vector.

$$\left[E_1^{out}, E_2^{out}, E_3^{out}\right]^T = MK^{in} = \frac{e^{i\varphi_1}}{3} \cdot \begin{pmatrix} 1 + e^{i(\Delta\varphi + 2\theta)} \\ e^{i\theta}(1 + e^{i\Delta\varphi}) \\ e^{i\theta}(1 + e^{i(\Delta\varphi + \theta)}) \end{pmatrix} \cdot E(t) \tag{5}$$

The measured intensities $I_n = |E_n^{out}|^2$ (n=1, 2, 3) of the three outputs are,

$$\begin{pmatrix} I_1 \\ I_2 \\ I_3 \end{pmatrix} = \frac{2I_0}{9} \begin{pmatrix} 1 + \cos(\Delta\varphi - 2\pi/3) \\ 1 + \cos(\Delta\varphi) \\ 1 + \cos(\Delta\varphi + 2\pi/3) \end{pmatrix} \tag{6}$$

where $I_0 = |E(t)|^2$ is the input intensity. Then the differential phase can be obtained.

$$\Delta\varphi = \arctan\left[\frac{\sqrt{3}(I_3 - I_1)}{I_3 + I_1 - 2I_2}\right] \tag{7}$$

2.2. Asymmetric 3 × 3 optical fiber coupler

However, the commercially available 3 × 3 optical fiber coupler is usually asymmetric and lossy. So the transmissivity of 3 × 3 coupler from port m to port n (m, n = 1, 2, 3) is $b_{mn}\exp(i\theta_{mn})$, where b_{mn} and θ_{mn} are the splitting ratio and phase delay of coupler, respectively. The forward transmission matrix of 3 × 3 coupler is then given by.

$$T_{3nm} = b_{nm} \exp(\mathrm{i}\theta_{nm}) \tag{8}$$

Similarly, the backward transmission matrix of 3 × 3 coupler is then given by,

$$T'_{3nm} = b'_{nm} \exp(\mathrm{i}\theta'_{nm}) \tag{9}$$

where b'_{mn} is the splitting ratio and θ'_{mn} is the phase delay of 3 × 3 coupler from port n to port m. The matrix of the two arms of the Michelson interferometer is given by,

http://dx.doi.org/10.5772/66129

$$P = \begin{pmatrix} p_{11} & 0 & 0 \\ 0 & p_{22}\exp(-i\omega\tau - i\delta) & 0 \\ 0 & 0 & 0 \end{pmatrix} \tag{10}$$

where p_{11} and p_{22} are the transmissivity of the two arms, respectively; τ and δ are the differential delay time and the differential phase delay between the signals in two arms of the Michelson interferometer. The operation of the whole interferometer is then described by the system matrix.

$$\begin{aligned} M_{nm} &= \left(T_3' P T_3\right)_{nm} \\ &= b'_{n1} p_{11} b_{1m} \exp\left[i\left(\theta'_{n1} + \theta_{1m}\right)\right] + b'_{n2} p_{22} b_{2m} \exp\left[i\left(\theta'_{n1} + \theta_{2m}\right)\right] \exp(-i\omega\tau - i\delta) \end{aligned} \tag{11}$$

The output light from the output port n is detected by a photodetector having a responsivity of r_n. The detected intensities from the output port n, I_n, can be expressed as.

$$\begin{aligned} I_n(t) &= r_n \left|E_n^{\text{out}}\right|^2 \\ &= r_n c_{n1}^2 \left|E(t)\right|^2 + r_n c_{n2}^2 \left|E(t-\tau)\right|^2 + \eta_n \cos(\delta + \Delta\varphi)\left|E(t)E(t-\tau)\right| + \\ &\quad \zeta_n \sin(\delta + \Delta\varphi)\left|E(t)E(t-\tau)\right| \end{aligned} \tag{12}$$

Define an intermediate matrix,

$$X' = \begin{pmatrix} X'_1(t) & X'_2(t) & X'_3(t) \end{pmatrix}^{\mathrm{T}} = \begin{pmatrix} \cos(\delta + \Delta\varphi)\left|E(t)E(t-\tau)\right| \\ \sin(\delta + \Delta\varphi)\left|E(t)E(t-\tau)\right| \\ \left(\left|E(t)\right|^2 + \left|E(t-\tau)\right|^2\right)/2 \end{pmatrix} \tag{13}$$

Then,

$$\begin{pmatrix} I_1(t) \\ I_2(t) \\ I_3(t) \end{pmatrix} = \begin{pmatrix} \eta_1 & \zeta_1 & \xi_1 \\ \eta_2 & \zeta_2 & \xi_2 \\ \eta_3 & \zeta_3 & \xi_3 \end{pmatrix} \begin{pmatrix} X'_1(t) \\ X'_2(t) \\ X'_3(t) \end{pmatrix} + \begin{pmatrix} r_1\left(c_{11}^2 - c_{12}^2\right) \\ r_2\left(c_{21}^2 - c_{22}^2\right) \\ r_3\left(c_{31}^2 - c_{32}^2\right) \end{pmatrix} \frac{\left|E(t)\right|^2 - \left|E(t-\tau)\right|^2}{2} \tag{14}$$

Where

$$\begin{aligned}
&\eta_n = 2r_n c_{n1} c_{n2} \cos\theta_n \\
&\varsigma_n = 2r_n c_{n1} c_{n2} \sin\theta_n \\
&\xi_n = r_n\left(c_{n1}^2 + c_{n2}^2\right) \\
&c_{nm} = p_{mm} b'_{nm} b_{m1} \\
&\theta_n = \left(\theta'_{n2} + \theta_{21}\right) - \left(\theta'_{n1} + \theta_{11}\right) \\
&\Delta\varphi = \varphi(t) - \varphi(t-\tau)
\end{aligned} \quad , \quad \begin{pmatrix} n = 1,2,3 \\ m = 1,2 \end{pmatrix} \tag{15}$$

The parameters η_n, ς_n, and ξ_n are constant for the setup, once the devices and structure are determined. They can be obtained by a broadband light source without measuring each parameter one by one as said in Ref. [15]. Eq. (13) can be transformed as.

$$X' = \begin{pmatrix} \eta_1 & \varsigma_1 & \xi_1 \\ \eta_2 & \varsigma_2 & \xi_2 \\ \eta_3 & \varsigma_3 & \xi_3 \end{pmatrix}^{-1} \begin{pmatrix} I_1(t) \\ I_2(t) \\ I_3(t) \end{pmatrix} - \begin{pmatrix} \eta_1 & \varsigma_1 & \xi_1 \\ \eta_2 & \varsigma_2 & \xi_2 \\ \eta_3 & \varsigma_3 & \xi_3 \end{pmatrix}^{-1} \begin{pmatrix} r_1\left(c_{11}^2 - c_{12}^2\right) \\ r_2\left(c_{21}^2 - c_{22}^2\right) \\ r_3\left(c_{31}^2 - c_{32}^2\right) \end{pmatrix} \frac{\left|E(t)\right|^2 - \left|E(t-\tau)\right|^2}{2} \tag{16}$$

Eq. (16) shows the relation between the differential phase $\Delta\varphi$ and the detectors outputs (I_1, I_2, I_3). We note that the second term on the right-hind side of Eq. (16) becomes zero or can be omitted under the following conditions: (a) the splitting ratios of the 3 × 3 coupler are uniform (i.e., $c_{n1} = c_{n2}$ for all n), or (b) the intensity of the laser under test is constant or periodical (i.e., $|E(t)|^2 - |E(t-\tau)|^2 = 0$), or (c) the extinction ratio of the Michelson interferometer. As a result, the differential phase $\Delta\varphi(t)$ accumulated in delay time τ can be obtained in the following simple form

$$\Delta\varphi(t) = \varphi(t) - \varphi(t-\tau) = \arctan\left(\frac{X'_2(t)}{X'_1(t)}\right) - \overline{\arctan\left(\frac{X'_2(t)}{X'_1(t)}\right)} \tag{17}$$

3. The application in laser noise measurement

3.1. Experimental setup

Based on the 120° phase difference technology, the experimental setup of laser noise measurement is shown in **Figure 2** [18]. It consists of a commercially available 3 × 3 optical fiber coupler (OC), a circulator (C), two Faraday rotator mirrors (FRMs), three photodetectors (PDs), a data acquisition board (DAC) or a digital oscilloscope, and a computer. The 120° phase difference Michelson interferometer is composed of the 3 × 3 coupler and the FRMs. On one hand, the FRM will remove the polarization fading caused by external disturbance on the two beam fibers of the interferometer. On the other hand, the length or index of the fiber configuring the interferometric arms would change randomly because of temperature fluctuations, vibration,

http://dx.doi.org/10.5772/66129

and other types of environmental disturbances; thus it induces low-frequency random-phase drifts in the interferometric signal. So in the proposed experimental setup, the complete interferometer is housed in an aluminum box enclosed in a polyurethane foam box for thermal and acoustic isolation. Meantime, the two fiber arms of the Michelson interforometer are placed closely in parallel to improve the stability against the perturbation.

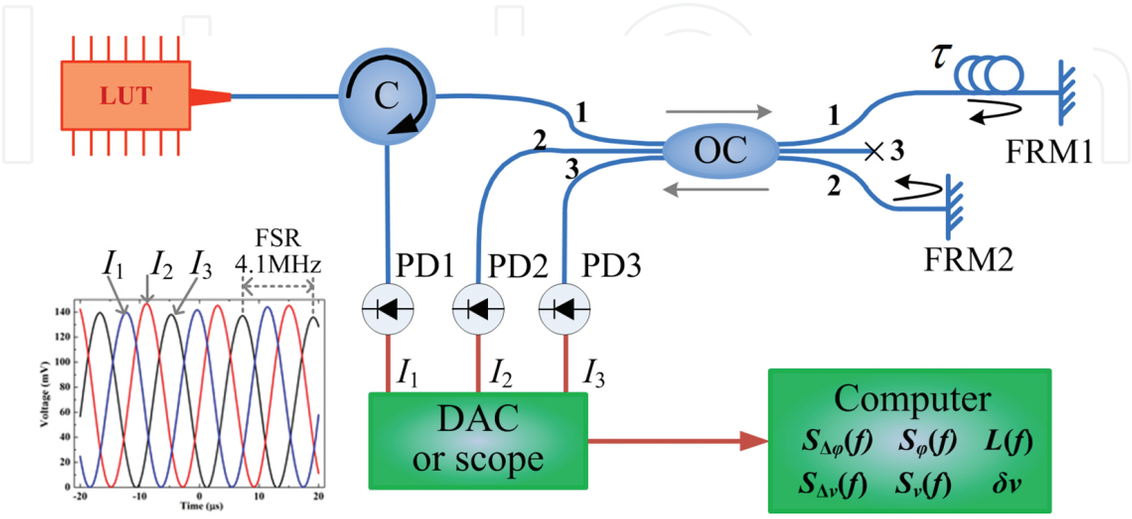

Figure 2. Experimental setup used to measure the laser phase and frequency noise, and the output interference fringe of the PD1, PD2, PD3 (inset). LUT: laser under test, C: circulator, OC: optical fiber coupler, FRM: Faraday rotation mirror, PD: photodetector, DAC: data acquisition board [18].

The laser under test (LUT) injects the left port 1 of the 3 × 3 optical fiber coupler through a circulator and then splits into three parts by the coupler. Two of them interfere mutually in the coupler after being reflected by Faraday mirrors and with different delay times, and the third part of them is made reflection-free. Then the interference fringes are obtained from the left port 1, 2, and 3 of the coupler and read by a DAC or a digital oscilloscope.

In the experimental setup, a swept laser source with linewidth of about 2.5 kHz [19] is used as the broadband light source to show clearly the small free spectral range (FSR) of the MI. The measured interference fringe is shown in the inset figure of **Figure 1**. On the other hand, all parameters of the devices are considered in the differential phase fluctuation calculation process, so the possible errors from device defects such as imperfect splitting ratio or phase difference are removed, and the requirements for the device performance parameters are also relaxed. In our experimental setup, the final setup parameters are τ = 244 ns (corresponding FSR of the MI is 4.1 MHz), and

$$\begin{pmatrix} \eta_1 & \varsigma_1 & \xi_1 \\ \eta_2 & \varsigma_2 & \xi_2 \\ \eta_3 & \varsigma_3 & \xi_3 \end{pmatrix} = \begin{pmatrix} 0.1198 & 0.0002 & 0.1223 \\ -0.0519 & 0.1366 & 0.1491 \\ -0.0634 & -0.1094 & 0.1290 \end{pmatrix} \tag{18}$$

When the setup parameters are calibrated, the whole setup is in a state of plug-and-play.

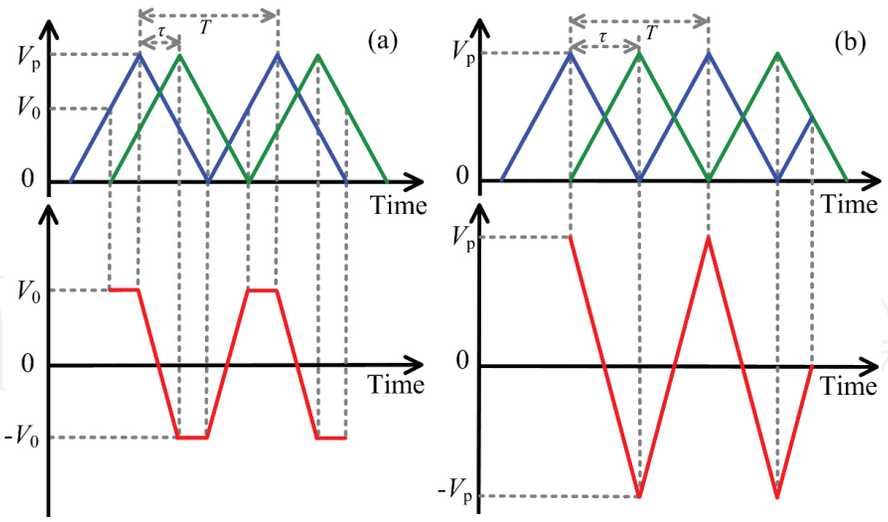

Figure 3. Demodulation principle of the setup for triangle waveforms with different modulation periods (a) $T \neq 2\tau$ and (b) $T = 2\tau$ [18].

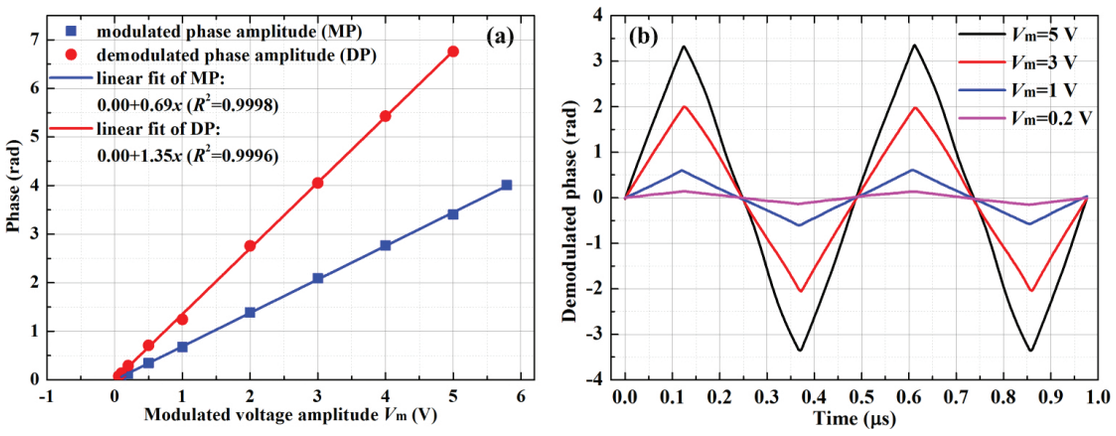

Figure 4. Modulated and demodulated (a) triangle phase amplitude and (b) waveform at different modulated voltage amplitudes [18].

To verify the correction of the phase demodulation of the setup, a demodulated test for a preset modulated phase by a LiNbO3 phase modulator is demonstrated. A narrow linewidth laser that is phase-modulated with the LiNbO3 phase modulator is used as LUT. The triangle waveform is selected to the modulation waveform for holding the frequency components as such and much more. Hence, the fact of the interference at the coupler is a subtraction between two triangle waveforms with delay time τ as shown in **Figure 3**. The modulation period T needs to be twice of the delay time difference τ. Otherwise, there are some constants in the interference fringe as shown in Figure 3(a), accordingly the triangle wave cannot be demodulated. Once the triangle waveform is demodulated correctly as shown in Figure 3(b), the demodulated amplitude would be twice the input modulated amplitude. **Figure 4**. shows the demodulated triangle phase amplitude and their waveforms at different modulated voltage amplitudes. The results confirmed the correction of the differential phase demodulation both

http://dx.doi.org/10.5772/66129

in terms of waveform and amplitude. **Figure 5** shows the time-domain interference fringes of the MI and the corresponding demodulated phase waveform at a fixed modulated voltage. The red curve and the black curve represent the results of two independent tests at different time, respectively. Despite the interference fringe changes at different time due to the environment variation, the demodulated phase would not change and hold the consistence with the input phase modulation, so the consistency and robustness of the proposed setup is verified.

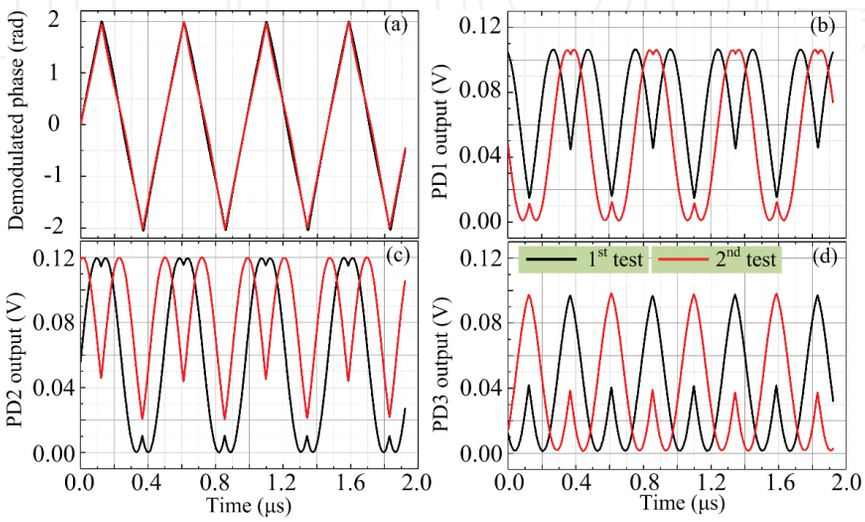

Figure 5. Output voltages of (b) PD1, (c) PD2, (d) PD3, and (a) corresponding demodulated phase waveforms at a fixed modulated voltage V_m = 3 V. The red and black lines represent the first and second test, respectively [18].

3.2. Laser noise theory

Considering the relation between the delay phase φ and frequency ν;

$$\varphi = 2\pi \frac{nl\nu}{c} = 2\pi\tau\nu \tag{19}$$

the differential phase variation is from the laser frequency variation in the time interval τ, because the delay time difference τ of the MI is fixed and the random variation of the fiber is eliminated carefully by some techniques as described above. So from the differential phase fluctuation $\Delta\varphi(t)$, the laser frequency fluctuation in time interval τ defined as differential frequency fluctuation $\Delta\nu(t)$ can be expressed as

$$\Delta\nu(t) = \Delta\varphi(t)/(2\pi\tau). \tag{20}$$

Hence, the PSD of differential phase fluctuation $\Delta\varphi(t)$ and differential frequency fluctuation $\Delta\nu(t)$ can be calculated, respectively, in the computer by PSD estimation method [20] and

denoted as $S_{\Delta\varphi}(f)$ and $S_{\Delta\nu}(f)$, respectively, where f is the Fourier frequency. Meantime, from the linearity of the Fourier transform, they have a fixed relation

$$S_{\Delta\nu}(f) = \left(\frac{1}{2\pi\tau}\right)^2 S_{\Delta\varphi}(f). \tag{21}$$

So far, the differential phase fluctuation $\Delta\varphi(t)$ accumulated in the delay time difference τ of the MI, corresponding differential frequency fluctuation $\Delta\nu(t)$, and their PSD is calculated. But these values are not the instantaneous information of the LUT. Furthermore, considering the relation of differential phase fluctuation $\Delta\varphi(t)$ and instantaneous phase fluctuation $\varphi(t)$ expressed in Eq. (17), the definition of the PSD [21], linearity, and time-shifting properties of Fourier transform, we derived strictly the PSD of laser instantaneous phase fluctuation and frequency fluctuation, which can be expressed as,

$$S_{\varphi}(f) = \frac{1}{4\left[\sin(\pi f\tau)\right]^2} S_{\Delta\varphi}(f) \tag{22}$$

.

$$S_{\nu}(f) = \frac{f^2}{4\left[\sin(\pi f\tau)\right]^2} S_{\Delta\varphi}(f) = \frac{1}{\left[\mathrm{sinc}(\pi f\tau)\right]^2} S_{\Delta\nu}(f) \tag{23}$$

From Eq. (22), the single-side-band phase noise can also be obtained with [22].

$$L(f) = \frac{1}{2} S_{\varphi}(f) = \frac{1}{8\left[\sin(\pi f\tau)\right]^2} S_{\Delta\varphi}(f) \tag{24}$$

Eq. (22) means that, at the low Fourier frequency domain, the PSD of the laser instantaneous phase fluctuation $S_{\varphi}(f)$ would be larger than the PSD of the differential phase fluctuation $S_{\Delta\varphi}(f)$, but at the high Fourier frequency domain, the former is smaller than the latter. Eq. (23) means that, however, the PSD of the laser instantaneous frequency fluctuation $S_{\nu}(f)$ is larger than the PSD of the differential frequency fluctuation $S_{\Delta\nu}(f)$ at any positive Fourier frequency. On the other hand, it is observed that if the differential phase and frequency fluctuation are normalized in 1 m delay fiber ($\tau \sim 5$ ns), then

$$S_{\nu}(f) \approx S_{\Delta\nu}(f), \quad \text{for } f < 5\,\text{MHz}. \tag{25}$$

http://dx.doi.org/10.5772/66129

Eq. (25) means that the PSD of the laser instantaneous frequency fluctuation $S_\nu(f)$ would approximately equal to the PSD of the differential frequency fluctuation $S_{\Delta\nu}(f)$ at the Fourier frequency less than MHz level. In physics, the results can be so explained that the frequency is the differential of the phase and the delay of the MI is equivalent to the differential operation for the phase. The conclusions are very important that the characterization of differential phase and instantaneous phase (laser phase) should be carefully distinguished, but the instantaneous frequency can be replaced by the differential frequency sometimes in the practical engineering applications.

3.3. Laser noise measurement results

First, the phase and frequency noise of an external-cavity semiconductor laser (RIO ORION™) [23] with a wavelength of 1551.7 nm and a linewidth of about 2 kHz are measured. The PSD of the differential phase fluctuation is normalized to 1 m delay fiber ($S_{\Delta\varphi}(f)$ @ 1 m), the PSD of the differential frequency fluctuation is normalized to 1 m delay fiber ($S_{\Delta\nu}(f)$ @ 1 m), and the PSD of instantaneous frequency fluctuation $S_\nu(f)$, the PSD of the instantaneous phase fluctuation $S_\varphi(f)$, and the laser phase noise $L(f)$ are shown in **Figure 6**. The data are very close to that given in the product datasheets or the typical data given in the website [23]. The curves clearly demonstrate the relations between these physical quantities as described above. At the focused frequency range (<1 MHz), $S_{\Delta\nu}(f)$ @ 1 m approximately equals to $S_\nu(f)$, $S_{\Delta\varphi}(f)$ @ 1 m is much less than $S_\varphi(f)$, and laser phase noise $L(f) = S_\varphi(f)/2$. So the usage of PSD of differential phase as the laser phase noise is not strictly correct and needs more careful definition and consideration.

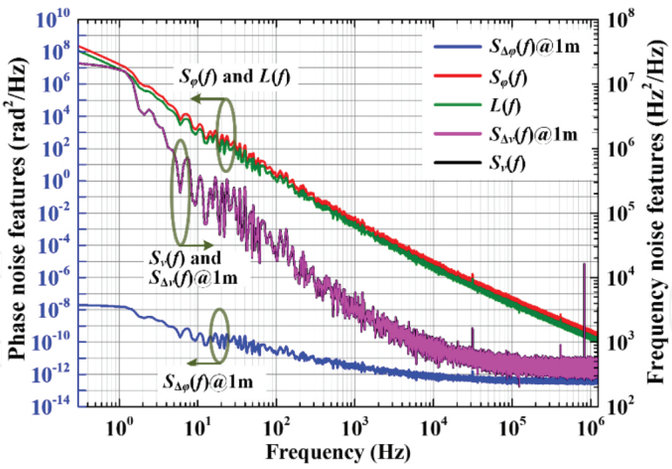

Figure 6. PSD of the differential phase fluctuation ($S_{\Delta\varphi}(f)$ @ 1 m), differential frequency fluctuation ($S_{\Delta\nu}(f)$ @ 1 m), instantaneous phase fluctuation $S_\varphi(f)$, instantaneous frequency fluctuation $S_\nu(f)$ and phase noise $L(f)$ of the RIO laser [18].

From the PSD of the frequency fluctuation $S_\nu(f)$, the linewidth at different observation time can be calculated. **Figure 7** shows the linewidth calculated with the approximated model presented in Ref. [24] for different values of the integration bandwidth. The results indicate that the linewidth is very dependent on the integration bandwidth. Linewidth would increase with the

increase of observation time (in other words, linewidth increases with the decrease of the lower limit of the integration bandwidth). It mainly results from the presence of the $1/f^{\alpha}$ type noise in the PSD of frequency fluctuation. In a high-frequency domain (>100 kHz), there is only white noise, and the minimum linewidth of about $\delta\nu_1 = 2$ kHz is calculated. Meantime, the inset figure shows the linewidth of the same laser measured by the self-delay heterodyne (SDH) method [14] with heterodyne frequency of 80 MHz and optical fiber delay length of 45 km. The Lorentz fitted linewidth at −20 dB from the spectrum measured by the SDH method is about 51.7 kHz, so the laser linewidth is about $\delta\nu_2 = 2.6$ kHz, and the fitted linewidth would not vary with the observation time. It indicates that the nonwhite noise components are not revealed in the Lorentz fitted results of SDH method, but the values are also conservative for white noise components and about 30% larger than the values calculated by the PSD of frequency fluctuation. This is because the tail of the spectrum measured by SDH method is not taken into consideration in the Lorentz fitting process, resulting in the fitted value being larger than the real value. Therefore, PSD of frequency fluctuation is recommended to completely describe the frequency noise behavior, and a specified linewidth value should be reported with the corresponding integration bandwidth or observation time.

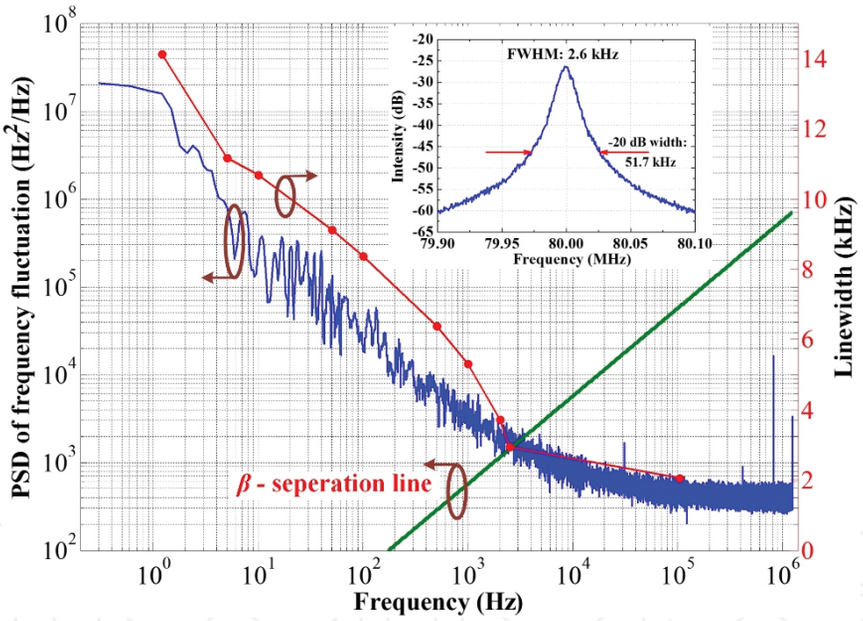

Figure 7. PSD of instantaneous frequency fluctuation of the RIO laser and the β – separation line given by $S_\nu(f) = 8\ln 2 f/\pi^2$ [24] (left axis), laser linewidth (FWHM) obtained by the method in Ref. [24] (right axis) and by the SDH method (inset) [18].

Second, the noise features of commercial distributed feedback (DFB) semiconductor laser are measured under different operating temperatures (24 and 22.7°C) and different operating currents (71, 91, 111, and 136 mA), shown in Figures 8 and 9. **Figure 8** shows that this DFB laser is more suitable for working at 24°C than at 22.7°C. **Figure 9** shows that the PSDs of frequency fluctuation $S_\nu(f)$ decrease with the increase of operating currents from 71 to 136 mA. According to above results, if we measure the PSDs of frequency fluctuation $S_\nu(f)$ of the laser

http://dx.doi.org/10.5772/66129

under a wide range of operating temperatures and currents, the optimum operating temperature and current can be found out.

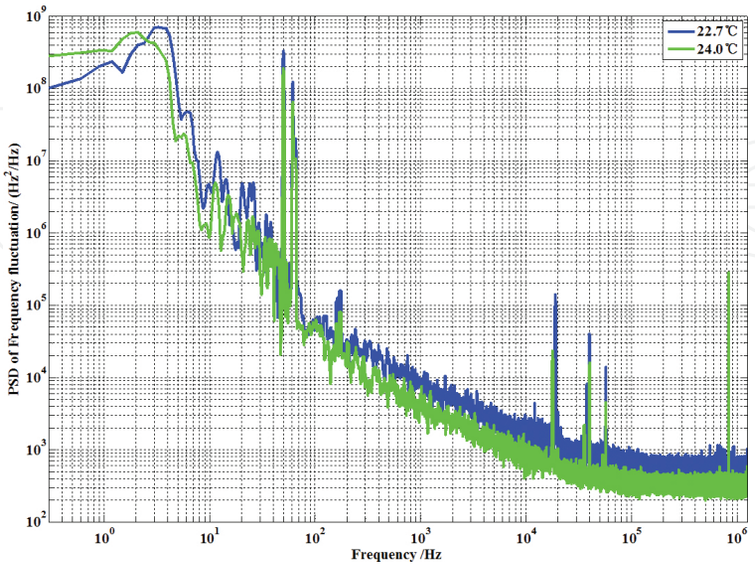

Figure 8. $S_{\nu}(f)$ of the DFB laser at operating temperature of 22.7 and 24.0°C.

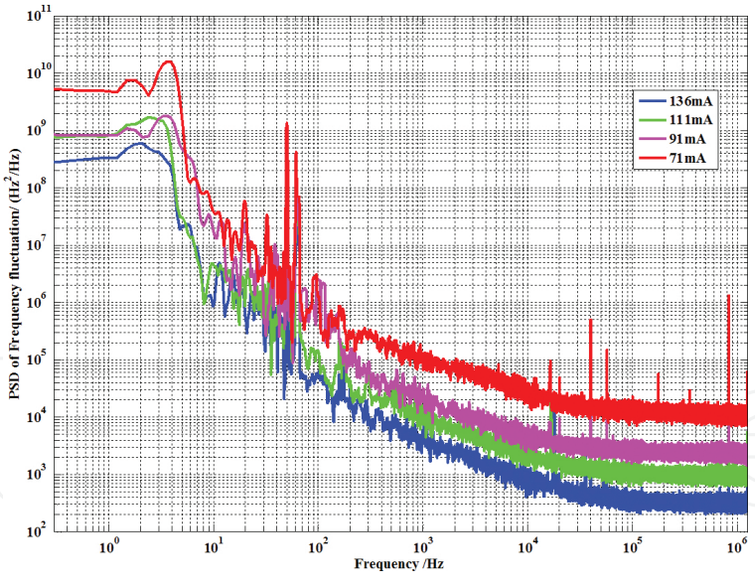

Figure 9. $S_{\nu}(f)$ of the DFB laser at operating current of 71, 91, 111, 136 mA.

4. The application in phase-sensitive OTDR

The experimental setup is shown in **Figure 10** [25]. The light source is a DFB laser with an output power of 20 mW and a wavelength of 1551.72 nm, which is injected into the acoustic-

optic modulator (AOM) to generate the pulses with a width of 40 ns and a repetition rate of 100 kHz. Before being injected into the fibre under test (FUT), the pulses would be amplified by the Erbium-doped fiber amplifier 1 (EDFA1). The backward Rayleigh scattering is amplified by the EDFA2 and then launched into the circulator2, and ASE noise of EDFA2 has been filtered by the fibre Bragg grating (FBG). Then the amplified scattering with better signal-to-noise ratio (SNR) is injected into one port of the 3 × 3 coupler through circulator3. There are two ports on the other side of the 3 × 3 coupler connected to FRMs and the other one port made reflection-free. The interferometer with 4 m delay is housed in a sealed box for thermal and acoustic isolation, avoiding disturbance from the environment. The fiber length between PDs and each coupler port is set as equal to guarantee the same optical path. A trichannel digital acquisition (DAQ) card is used to acquire the voltage signal, and a radio frequency driver (RFD) is used to trigger the AOM and DAQ card simultaneously for synchronization. The collected trichannel signals are processed by the software program to demodulate phase information by using Eq. (16).

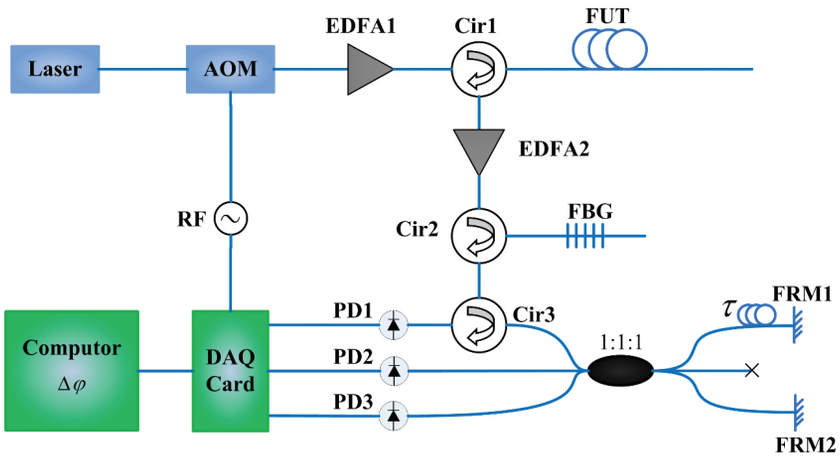

Figure 10. Experimental setup used to demodulate the distributed phase in φ-OTDR [25].

Phase sensitive optical time domain reflectometer (φ-OTDR) based on 120° phase difference Michelson interferometer is a new demodulation scheme used to demodulate the distributed phase. The 120° phase difference interferometer φ-OTDR can detect the phase along a 3 km fiber and the acoustic signal within the whole human hearing range from 20 Hz to 20 kHz is reproduced accurately and fast. The results show that the scheme has high accuracy and real-time response. The acoustic vibration system can be used in audio monitoring, and the health and state monitoring of railway or other structures [25].

5. Conclusion

A laser phase and frequency noise measurement technique based on a 120° phase difference unbalanced Michelson interferometer composed of a 3 × 3 optical fiber coupler and two Faraday rotator mirrors is proposed. In the method, the laser differential phase fluctuation

accumulated by the interferometer delay time is demodulated directly at first and then the phase and frequency noise is calculated by the PSD estimation for the differential phase. Also the concepts and differences of differential phase and frequency fluctuation PSDs, instantaneous phase and frequency fluctuation PSDs, and phase noise are defined strictly and discussed carefully. The method can obtain the noise features of a narrow linewidth laser without any specific assumptions or noise models. Meantime, the technique is used to characterize a narrow linewidth external-cavity semiconductor laser, which confirmed the correction of the method and revealed the fact that the linewidth would increase with the increase of observation time, and the Lorentz fitted linewidth measured by the SDH method only includes the contribution of the white noise components and would be larger than the real value. Moreover, the technique can monitor the state change of commercial DFB semiconductor lasers in different processes of designing, installation, debugging, routine test, and final check test, and it offers suggestions to optimize design and improve its performance. The 120° phase difference technology is also applied to test the phase difference between Rayleigh scattering in phase sensitive optical time domain reflectometer (φ-OTDR).

Author details

Yang Fei[1*], Xu Dan[1,2], Cai Haiwen[1] and Qu Ronghui[1]

*Address all correspondence to: fyang@siom.ac.cn

1 Shanghai Institute of Optics and Fine Mechanics, Chinese Academy of Sciences, Shanghai, China

2 LNE-SYRTE, Observatoire de Paris, Paris, France

References

[1] M Trobs, L D'arcio, G Heinzel, et al. Frequency stabilization and actuator characterization of an ytterbium-doped distributed-feedback fiber laser for LISA. J. Opt. Soc. Am. B, 2009, 26(5): 1137–1140.

[2] O Lopez, A Haboucha, F Kéfélian, et al. Cascaded multiplexed optical link on a telecommunication network for frequency dissemination. Opt. Express, 2010, 18(16): 16849–16857.

[3] K Predehl, G Grosche, S M F Raupach, et al. A 920-kilometer optical fiber link for frequency metrology at the 19th decimal place. Science, 2012, 336(6080): 441–444.

[4] M Fujieda, M Kumagai, S Nagano, et al. All-optical link for direct comparison of distant optical clocks. Opt. Express, 2011, 19(17): 16498–16507.

[5] N Chiodo, K Djerroud, O Acef, et al. Lasers for coherent optical satellite links with large dynamics. Appl. Opt., 2013, 52(30): 7342–7351.

[6] F Lienhart, S Boussen, O Carraz, et al. Compact and robust laser system for rubidium laser cooling based on the frequency doubling of a fiber bench at 1560 nm. Appl. Phys. B-Lasers O., 2007, 89(2–3): 177–180.

[7] G A Cranch, G M H Flockhart, C K Kirkendall. Distributed feedback fiber laser strain sensors. IEEE Sens. J., 2008, 8(7–8): 1161–1172.

[8] J P Cariou, B Augere, M Valla. Laser source requirements for coherent lidars based on fiber technology. C. R. Phys., 2006, 7(2): 213–223.

[9] F Yang, Q Ye, Z Q Pan, et al. 100-mW linear polarization single-frequency all-fiber seed laser for coherent Doppler lidar application. Opt. Commun., 2012, 285(2): 149–152.

[10] H Lee, M G Suh, T Chen, et al. Spiral resonators for on-chip laser frequency stabilization. Nat. Commun., 2013, 4: 1–6.

[11] H Tsuchida. Laser frequency modulation noise measurement by recirculating delayed self-heterodyne method. Opt. Lett., 2011, 36(5): 681–683.

[12] T Okoshi, K Kikuchi, A Nakayama. Novel method for high resolution measurement of laser output spectrum. Electron. Lett., 1980, 16(16): 630–631.

[13] O Llopis, P H Merrer, H Brahimi, et al. Phase noise measurement of a narrow linewidth CW laser using delay line approaches. Opt. Lett., 2011, 36(14): 2713–2715.

[14] S Piazzolla, P Spano, M Tamburrini. Characterization of phase noise in semiconductor lasers. Appl. Phys. Lett., 1982, 41(8): 695–696.

[15] Y Takushima, H Y Choi, Y C Chung. Measurement of differential phasor diagram of multilevel DPSK signals by using an adjustment-free delay interferometer composed of a 3 × 3 optical coupler. J. Lightwave Technol., 2009, 27(6): 718–730.

[16] S K Sheem. Optical fiber interferometers with [3 × 3] directional couplers: Analysis. J. Appl. Phys., 1981, 52(6): 3865–3872.

[17] T Butler, S Slepneva, B O'shaughnessy, et al. Single shot, time-resolved measurement of the coherence properties of OCT swept source lasers. Opt. Lett., 2015, 40(10): 2277–2280.

[18] D Xu, F Yang, D J Chen, et al. Laser phase and frequency noise measurement by Michelson interferometer composed of a 3 × 3 optical fiber coupler. Opt. Express, 2015, 23(17): 22386–22393.

[19] F Wei, B Lu, J Wang, et al. Precision and broadband frequency swept laser source based on high-order modulation-sideband injection-locking. Opt. Express, 2015, 23(4): 4970–4980.

[20] J Rutman. Characterization of phase and frequency instabilities in precision frequency sources: fifteen years of progress. Proc. IEEE, 1978, 66(9): 1048–1075.

[21] P D Welch. The use of fast Fourier transform for the estimation of power spectra: a method based on time averaging over short, modified periodograms. IEEE Trans. Audio Electro., 1967, 15(2): 70–73.

[22] R P Scott, C Langrock, B H Kolner. High-dynamic-range laser amplitude and phase noise measurement techniques. IEEE J. Sel. Top. Quant., 2001, 7(4): 641–655.

[23] Rio Orion™ Laser Module. http://www.rio-inc.com/_products/orion.html.

[24] G D Domenico, S Schilt, P Thomann. Simple approach to the relation between laser frequency noise and laser line shape. Appl. Opt., 2010, 49(25): 4801–4807.

[25] Y L Cao, Y Fei, D Xu, et al. Phase sensitive OTDR based on 120° phase difference Michelson interferometer. Chin. Phy. Lett., 2016, 33(05): 050701.

IntechOpen